Symmetry Properties of Vibrational Modes in Mesoporphyrin IX Dimethyl Ester Investigated by Polarization-Sensitive Resonance Raman and CARS Spectroscopy

J. Koster,[†] J. Popp,[‡] W. Kiefer,[†] and S. Schlücker*,[†]

Institut für Physikalische Chemie, Julius-Maximilians-Universität Würzburg, Am Hubland, 97074 Würzburg, Germany, and Institut für Physikalische Chemie, Friedrich-Schiller-Universität Jena, Helmholtzweg 4, 07743 Jena, Germany

Received: May 10, 2006; In Final Form: August 2, 2006

The symmetry properties of selected vibrational modes of mesoporphyrin IX dimethyl ester (MP-IX-DME) in solution are investigated under different electronic resonance conditions. The Raman band parameters of the macrocycle modes ν_2, ν_{10}, ν_{11}, and ν_{19} are determined from a quantitative analysis of polarized spontaneous resonance Raman (RR) and polarization-sensitive (PS) multiplex coherent anti-Stokes Raman scattering (CARS) spectra obtained with pre-resonant *B* band and resonant Q_x band excitation, respectively. Additionally, the molecular geometry and the vibrational modes of MP-IX-DME are calculated by employing density functional theory (DFT) on the B3LYP/6-31G(d) level. Both the DFT-derived structure and the Raman spectroscopic parameters of MP-IX-DME indicate minor deviations from an ideal D_{2h} macrocycle symmetry. To assess the influence of the β substitution pattern on the in-plane symmetry, calculated normal-mode vectors and several experimentally detected parameters, such as peak positions, depolarization ratios, and coherent phases, are analyzed. The effects of the macrocycle substitution pattern are different for the selected vibrational modes: ν_2 in particular is very sensitive to subtle perturbations of the in-plane symmetry. The considerable activity of totally symmetric vibrations observed in the PS CARS spectra of MP-IX-DME and the correlation of mode symmetries with coherent phases confirm earlier PS CARS results on octaethylporphine (OEP) acquired under the same electronic resonance conditions.

1. Introduction

Structural investigations of free-base porphyrins are important because of their role as building blocks for a large number of biologically relevant molecules. Among other techniques for studying porphyrins in solution, resonant Raman techniques have been widely used.[1−4] Besides spontaneous Raman spectroscopy, coherent four-photon Raman techniques can also be applied for that purpose.[5−12] One major advantage of the coherent techniques is that excessive fluorescence, which often occurs when exciting porphyrins in the low-energy electronic absorption range, can be spatially, and in coherent anti-Stokes processes also spectrally, separated from the Raman-resonant signals. Combining coherent four-photon spectroscopies with a polarization-sensitive measurement scheme[13−19] and an appropriate quantitative line shape analysis[7,8] further allows effective resolution of distinct components of the third-order susceptibility tensor $\chi^{(3)}$ and consequent determination of a complete set of Raman band parameters. In addition to Raman spectroscopic techniques, density functional theory (DFT)-based calculations can also be employed to obtain valuable information about the structural and vibrational properties of porphyrins.[20−22] The focus of this work, however, lies in the interpretation of the results from nonlinear Raman spectroscopy, which is supported by data from linear Raman spectroscopy and DFT calculations.

In the current study, we apply polarization-sensitive (PS) coherent anti-Stokes Raman scattering (CARS) spectroscopy to investigate mesoporphyrin IX dimethyl ester (MP-IX-DME) in solution. For comparison purposes, polarized spontaneous Raman spectra of MP-IX-DME are also recorded. Furthermore, a DFT-based geometry optimization and normal-mode calculation are carried out to assist the spectroscopic interpretation. The coherent Raman spectra are measured with an excitation condition that involves a 2-fold electronic resonance in the Q_x absorption region. In contrast, the spontaneous Raman spectra are recorded with an excitation wavelength that is pre-resonant to the strong *B* absorption band; under these conditions, the amount of fluorescence overlaying the spectra is still tolerable. Spontaneous Raman spectra have already been obtained in previous studies for MP-IX-DME with *B* and Q_y band excitation[23,24] and just recently for MP-IX in its free-acid form with excitation in the *B* band maximum.[22,25] In contrast to the study by Jarzęcki and Spiro[22] which focuses on the investigation of low-wavenumber vibrations to monitor out-of-plane distortions of the porphyrin macrocycle, our study examines the spectral region 1510−1670 cm^{-1} in detail where usually core-size marker bands are observed.

One main goal of our investigations is to reveal the influence of the β substitution pattern on the symmetry of the porphyrin macrocycle. In this context, we will compare the results presented here for the unsymmetrically substituted MP-IX-DME to our theoretical and Raman spectroscopic results on the symmetrically substituted octaethylporphine (OEP).[11,12] This comparison is also intended to examine how far the observed Raman spectroscopic behavior can be correlated to the DFT-derived data. Furthermore, our work is aimed to probe free-base porphyrins with excitation conditions that have not been extensively addressed before. Only a few studies are reported

* To whom correspondence should be addressed. E-mail: sebastian.schluecker@mail.uni-wuerzburg.de.
[†] Julius-Maximilians-Universität Würzburg.
[‡] Friedrich-Schiller-Universität Jena.

10.1021/jp062864y CCC: $33.50
Published on Web 09/13/2006

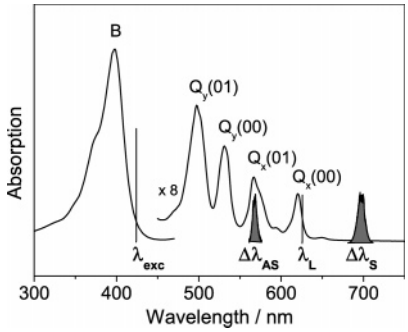

Figure 1. Absorption spectrum of a ~1 mM solution of mesoporphyrin IX dimethyl ester (MP-IX-DME) in CH_2Cl_2 together with the wavelength arrangement used in the RR and RCARS experiments and the molecular structure of MP-IX-DME (inset). Spontaneous Raman spectra were recorded with $\lambda_{exc} = 424.0$ nm. For the PS CARS experiments, a narrow-band pump laser at $\lambda_L = 625.7$ nm and a broad-band Stokes laser with $\Delta\lambda_S$ centered at 1630 cm^{-1} relative to λ_L were used as excitation sources; anti-Stokes signals were generated in the range of $\Delta\lambda_{AS}$.

where wavenumber-resolved coherent Raman spectroscopy has been applied to acquire spectra of free-base porphyrin systems with Q_x band excitation.[7,12] The current study on MP-IX-DME expands the data available for free-base porphyrins. This new information could be helpful in interpreting the underlying electronic coupling mechanisms which may differ from those known for metalloporphyrins. Finally, it should be stressed again that the application of a coherent Raman technique is essential to gain vibrational spectroscopic information on free-base porphyrins under Q_x band excitation conditions, because linear Raman techniques fail in this case due to excessive fluorescence signals.

2. Experimental Section

Computational Methods. Calculations were performed using DFT with the Becke−Lee−Yang−Parr composite exchange-correlation functional (B3LYP) and the 6-31G(d) basis set as implemented in the *Gaussian 03* (revision C.02) program package.[26]

Raman Spectroscopic Techniques. MP-IX-DME was purchased from Frontier Scientific (Logan, UT) and used without further purification. For the measurements, solutions of ~5 mM (for RCARS) and ~1 mM (for RR experiments) in dichloromethane, CH_2Cl_2, were prepared. Sample integrity was checked spectrophotometrically (Perkin-Elmer Lambda 19) before and after the experiments. The electronic absorption spectrum in the range 300−750 nm is depicted in Figure 1 for a ~1 mM solution of MP-IX-DME in dichloromethane. Absorption spectra of ~5 mM solutions (not shown) were also measured; the shape of the absorption curve of ~5 mM solutions is exactly the same as for ~1 mM solutions, with the absorption being stronger by a factor of approximately 5. This suggests a linear concentration dependence according to the Lambert−Beer law, implying that the UV−vis spectra are therefore usable to monitor the sample integrity. In addition to the UV−vis spectra, we also used the Raman spectra for direct monitoring of the sample integrity and to exclude the presence of aggregated porphyrin forms and/or degradation products. In case of the spontaneous Raman spectra, the amount of fluorescence was taken as a measure of the sample integrity; this amount remained nearly equally low during the required measurement time. In case of the CARS measurements, in which fluorescence is inherently not detected, control spectra at a certain analyzer position were taken at the beginning and the end of a polarization-sensitive measurement cycle; the line shapes of these control spectra were found to be identical, suggesting that the sample remained intact, since typical porphyrin decomposition products give rise to additional Raman bands in the investigated spectral region (1510−1670 cm^{-1}).

Spontaneous RR spectra were measured using the output of a dye laser (Coherent model 590; Stilbene 3 filled) that was pumped by an Ar^+ laser (Spectra Physics BeamLok 2085) operated in the UV multimode (333−364 nm). The excitation wavelength from the dye laser was tuned to $\lambda_{exc} = 424.0$ nm with ~50 mW output power. The sample was kept in a rotating cell[27] to minimize the required sample volume and to avoid photodegradation. The scattered light was collected in a 90° geometry by a 1:0.7/50 mm lens (Fuji Photo Optical lens CF50L) and focused on the entrance slit of a double monochromator (Spex 1404, 2400 gr/mm) equipped with a CCD camera (Photometrics SDS9000). The entrance slit was kept at a resolution of ~0.7 cm^{-1}. The polarization properties were controlled by using a Glan-Thompson polarizer and a double Fresnel rhomb before the sample and another Glan-Thompson polarizer as analyzer behind the sample. The maximum possible accuracy for the determination of depolarization ratios with this setup was estimated to be ±0.05 from measurements on CCl_4; this error estimate is also applied to the spontaneous Raman spectra of MP-IX-DME for spectrally well-separated bands (see Table 4). The MP-IX-DME spectra were recorded using the scanning multichannel technique (SMT);[28] for the desired spectral range, an overall measurement time of ~20 min was required for the parallel and perpendicular components. The sample solutions were prepared freshly before use, because slight sample degradation was detected over a period of several hours, recognizable by increasing fluorescence signals in the spectra.

Details of the nanosecond multiplex CARS setup, that was used to obtain the resonance CARS (RCARS) spectra, are given elsewhere.[29] In short, a Nd:YAG laser (Spectra Physics Quanta Ray GCR-4, 10 Hz, 7−8 ns; equipped with Spectra Physics Harmonic Generator HG-4) was used to synchronously pump two dye lasers. One dye laser (Molectron DL200, R101 filled) was operated in narrow-band mode to provide the pump wavelength $\lambda_L = 625.7$ nm. The second dye laser (Spectra Physics PDL3, Pyridine 1 filled) was operated in broad-band mode providing the Stokes continuum, $\Delta\lambda_S$, between ~685 and ~708 nm with a full width at half-maximum (FWHM) of ~220 cm^{-1} and a center position of ~1630 cm^{-1} relative to the pump wavelength. The pump and Stokes pulses were adjusted by a delay line for temporal overlap and focused onto the sample under an appropriate phase-matching angle by means of an achromatic lens. The sample was kept in a quartz capillary with plain windows and an inner diameter of 300 μm. The comparably short sample length minimizes reabsorption effects and lowers the attenuation of signal efficiency which occurs in multiplex CARS spectroscopy due to phase-mismatch.[30] The anti-Stokes continuum, $\Delta\lambda_{AS}$, was then collimated by a second achromatic lens, separated from the pump and the Stokes beams by means of an aperture, and focused on the entrance slit of a double monochromator (Spex 1403, 1800 gr/mm) equipped with a CCD camera (Photometrics SDS9000). The spectra were recorded using the SMT technique.[28] Under the experimental conditions, the FWHM of the pump laser was determined to be ~1.7 cm^{-1}, which can be considered the maximum possible resolution for the setup.

The control of the polarization conditions for the PS RCARS spectra is achieved as follows. Pump and Stokes beams are prepolarized by Glan-Thompson polarizers and are then each

passing a double Fresnel rhomb. The collimated anti-Stokes signal is viewed through a Glan-Thompson polarizer that serves as analyzer. The analyzer is kept in a fixed position while the desired polarization conditions are accomplished by simultaneously tuning the two double Fresnel rhombs. This avoids the necessity to make corrections for the polarization sensitivity of the detection system. However, the polarization characteristics of the optics that are mounted between polarizers and analyzer must be considered. Slight deviations from ideal linear beam polarizations, that occurred due to these optics, could be incorporated by appropriate correction parameters into the quantitative fitting procedure of the data. The experimental realization and the fitting procedure were checked on neat benzene in the spectral region of interest; the spectra of benzene contain two overlapping Raman bands (with $\rho \approx 0.75$) in this region and exhibit a signal-to-noise ratio similar to that of the MP-IX-DME spectra. Therefrom, overall accuracies of ± 0.15 for the determination of depolarization ratios (provided that the bands are approximately depolarized, i.e., $\rho \approx 0.75$) and $\pm 15°$ for the determination of coherent phases were estimated in the presented spectra.

Line Shape Analysis. To perform a reasonable quantitative evaluation of the spontaneous RR spectra, an appropriate baseline had to be subtracted from the original spectra to account for a small amount of underlying fluorescence. The parallel and perpendicular polarization components were then fitted simultaneously in the region 1510−1670 cm^{-1}, assuming four bands with pure Lorentzian profiles and a linear baseline for the parallel as well as for the perpendicular component.

The normalization procedure and the polarization scheme used for the PS CARS experiments have been explained in detail previously.[12] In short, an angle of $\alpha = 60°$ was chosen between the polarization directions of the pump and the Stokes laser. The spectra were recorded for six different analyzer angles $\beta = -30°, -60°, 90°, 60°, 30°$, and 0° which resolves the following components and linear combinations of the $\chi^{(3)}$ scattering tensor: $(\chi^{(3)}_{1111} + \chi^{(3)}_{1221})$, $(\chi^{(3)}_{1111} + 3\chi^{(3)}_{1221})$, $\chi^{(3)}_{1221}$, $(\chi^{(3)}_{1111} - 3\chi^{(3)}_{1221})$, $(\chi^{(3)}_{1111} - \chi^{(3)}_{1221})$, and $\chi^{(3)}_{1111}$, respectively. The normalization of the sample spectra was carried out by using the nonresonant background signal of the pure solvent (CH_2Cl_2). The normalized sample spectra were then fitted simultaneously with respect to the following expression that describes the dispersion of the CARS signal intensity, $I_{CARS}(\omega_{AS})$:[8,31]

$$I_{CARS}(\omega_{AS}) \propto \left| p^{NR}\chi^{(3)NR} + p^{E}\chi^{(3)E}\exp(i\Theta^{E}) + \sum_t p_t^{R} \frac{A_t^{R}\exp(i\Theta_t^{R})}{\Omega_t - (\omega_L - \omega_S) - i\Gamma_t/2} \right|^2 \quad (1)$$

with the configuration factors

$$p^{NR,E,R} = [(1 - \rho^{NR,E,R})\cos\alpha\cos\beta + \rho^{NR,E,R}\cos(\alpha + \beta)] \quad (2)$$

These two equations are central to the evaluation process; by setting β to the appropriate experimentally used values, they allow the simultaneous fit of several spectra measured with different polarization conditions.[7,8,12] This model assumes Lorentzian line functions for the Raman resonant contributions. The parameters Ω_t, A_t^R, Γ_t, Θ_t^R, and ρ_t^R denote the angular frequency, amplitude, line width, coherent phase, and depolarization ratio of the tth Raman mode, respectively; $(\omega_L - \omega_S)$ reflects the detuning of the Stokes frequency versus the pump frequency; nonresonant contributions are summarized in $\chi^{(3)NR}$ and purely electronically resonant contributions in $\chi^{(3)E}$. For the spectra on MP-IX-DME, a possible influence of purely electronic susceptibility, $\chi^{(3)E}$, was considered to be negligible, since a CH_2Cl_2 solvent mode at ~1423 cm^{-1} (not shown) was found to show no significant shift in coherent phase if measured on either pure solvent or the sample solution. The depolarization ratio of the nonresonant background could be fixed in the fitting process to the value of $\rho^{NR} = 1/3$, which is consistent with the Kleinman symmetry.[32] In principle, the analysis of four CARS spectra measured with different analyzer angles is sufficient for determining all parameters in eqs 1 and 2; the use of additional spectra as in our case, however, improves the accuracy of the curve fitting procedure.

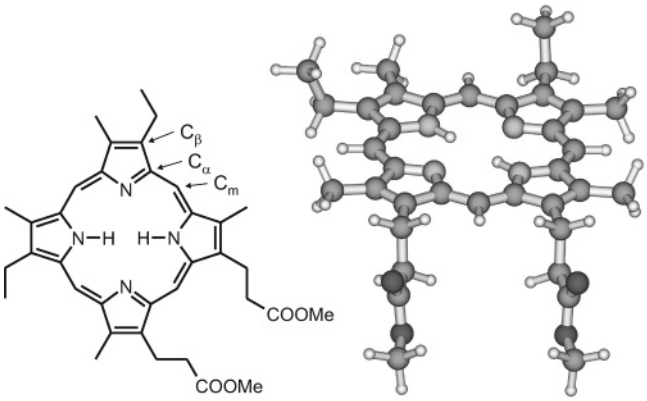

Figure 2. Geometry of mesoporphyrin IX dimethyl ester (right), optimized using DFT on the B3LYP/6-31G(d) level and the constitution formula (left) including the atom labeling as used in Table 1.

TABLE 1: Average Values of Selected Bond Lengths (Å) and Angles (deg) for the Porphyrin Macrocycle of MP-IX-DME and Other Free-Base Porphyrins

	exptl[a] MP-IX-DME	calcd MP-IX-DME	calcd[b] OPE	calcd[c] MP-IX	calcd[c] FBP
$C_\alpha-N$	1.366	1.366	1.366	1.368	1.368
$C_\alpha-C_\beta$	1.448	1.457	1.457	1.458	1.448
$C_\beta-C_\beta$	1.364	1.374	1.375	1.376	1.364
$C_\alpha-C_m$	1.388	1.397	1.397	1.398	1.397
$C_\alpha-N-C_\alpha$	107.8	108.1	108.1	108.0	108.1
$N-C_\alpha-C_m$	125.0	125.2	125.2	125.1	125.5
$C_\alpha-C^m-C_\alpha$	127.7	127.6	127.8	127.9	127.1
$C_\alpha-C_\beta-C_\beta$	107.0	106.7	106.7	106.7	107.1

[a] X-ray data from ref 34. [b] Adopted from ref 11. [c] Adopted from ref 22.

3. Results and Discussion

Density Functional Calculations. During the geometry optimization of MP-IX-DME, the tetrapyrrole macrocycle was restricted to a planar conformation because the planar core represents one among several stable conformations that can be calculated for metalloporphyrins[33] and free-base porphyrins.[22] It is also the most probable conformer to be experimentally detected in measurements on porphyrin solutions where no particular coordination effects on the macrocycle have to be considered.[33] The optimized geometry of MP-IX-DME is displayed in Figure 2, and selected bond parameters are listed in Table 1; the values are compared with corresponding data from the X-ray structure of MP-IX-DME and from calculations on other free-base porphyrins, namely, octaethylporphine (OEP), mesoporphyrin IX in its free-acid form (MP-IX), and free-base porphine (FBP). In contrast to the monomeric form that is used in the calculations, the crystallographic data[34] of MP-IX-DME exhibit two molecules per unit cell that are coordinated via two

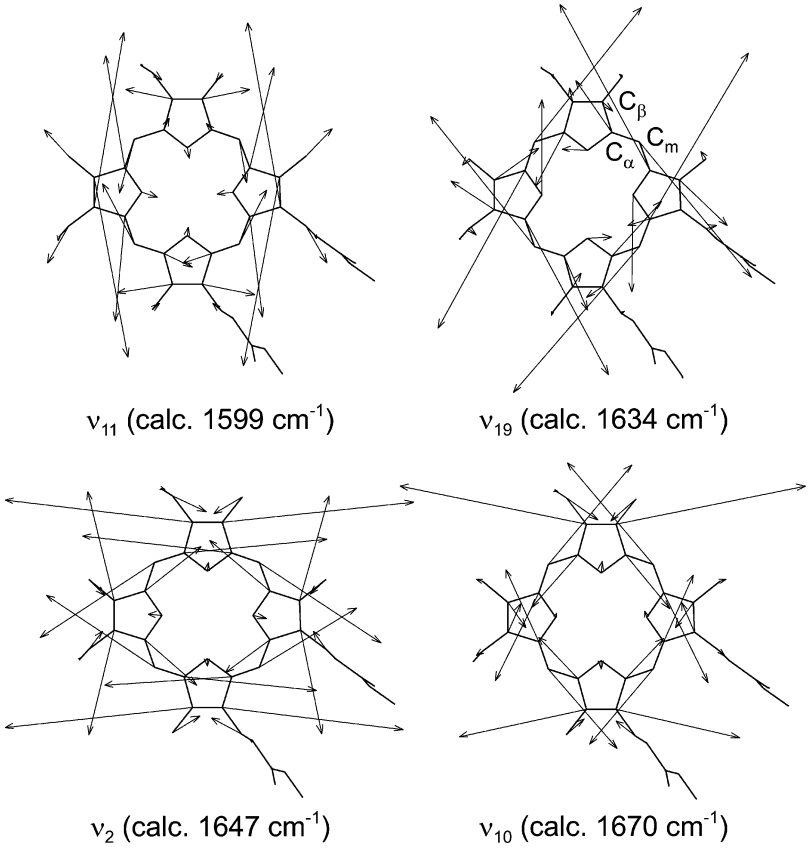

Figure 3. Calculated normal-mode vectors for selected macrocycle modes of MP-IX-DME. Protonated pyrrole rings are aligned horizontally in the presentation (protons not shown). The calculated harmonic wavenumbers are unscaled. The lengths of the vectors are only relative and do not reflect the absolute displacements of the atoms.

ester functionalities; although such coordination may also occur in our spectroscopic experiments on the dissolved substance, its effect on the macrocycle geometry should be negligible because of the large distance between the ester groups and the macrocycle. Apart from some very small deviations, the calculated core structure of MP-IX-DME is essentially the same as that determined experimentally and those calculated for other free-base porphyrins (see Table 1). Significant distortions from a D_{2h} symmetry cannot be identified. While the influence of β substituents on the macrocycle geometry is small, their influence on mode wavenumbers and resonance Raman intensities may, however, be considerable. A detailed study covering this aspect for MP-IX has just recently been published,[22] demonstrating that the substitution pattern has an impact on both in-plane and out-of-plane modes. That study focuses on the investigation of out-of-plane modes, which are usually found below 1000 cm^{-1}, to experimentally monitor corresponding macrocycle distortions; in contrast, our study examines in-plane modes above 1400 cm^{-1}, which are known to be sensitive to the porphyrin core size[22,35] and may therefore reveal subtle in-plane distortions.

In our linear and nonlinear Raman spectroscopic experiments, we examine macrocycle modes in the interval 1510−1670 cm^{-1}. The calculated eigenvectors of the four porphyrin modes in this spectral region are depicted in Figure 3. The assignment of the eigenvectors to the corresponding vibrational modes was accomplished through qualitative comparisons with several previously published calculations on free-base porphyrins.[11,20,21,36] Under strict D_{2h} conditions, ν_{11}, ν_2, and ν_{10} are a_g symmetric, while ν_{19} is b_{1g} symmetric. In a previous study on the fully symmetrically substituted OEP,[11] we found that the calculated eigenvectors of these modes completely reflect the corresponding symmetries. For MP-IX-DME, however, some small deviations can be recognized by analyzing the symmetry properties of the displacement eigenvectors (see Figure 3). In the case of ν_{10}, for example, the maximum displacement of the $C_\beta C_\beta$ stretch components at two opposite pyrrole rings is not exactly equal. A similar effect is observed for the $C_\beta C_\beta$ stretch components of ν_{19}. For the modes ν_{11} and ν_2, analogous effects are more obviously located at $C_\alpha C_m$ stretch components. As can be seen qualitatively from Figure 3, the strongest displacements, however, occur for $C_\beta C_\beta$ stretch motions in ν_{11} and ν_2, and for $C_\alpha C_m$ stretch motions in ν_{19} and ν_{10}, which is consistent with calculations on FBP.[21,36] In general, the observable deviations from ideal D_{2h} symmetry can be correlated to the specific β substitution pattern of MP-IX-DME. Due to this substitution pattern, no symmetry element is kept for the complete molecule. Furthermore, the propionic ester substituents differ significantly in mass from the other substituents. This obviously gives rise to recognizable effects on macrocycle vibrations. Moreover, these effects of the substitution pattern are not only restricted on the directly connected C_β atoms, but in some cases also concern the more remote C_α and C_m atoms.

The above discussion has shown that the qualitative examination of calculated normal-mode eigenvectors of MP-IX-DME already reveals slight in-plane deviations from an ideal D_{2h} macrocycle symmetry behavior, which were not obvious from the molecular structure.

Spontaneous Resonance Raman Spectroscopy. Polarized spontaneous RR spectra in the region 1300−1670 cm^{-1} are shown in Figure 4; the observed Raman bands are assigned to the following modes: ν_{20} (b_{1g}), ν_4 (a_g), ν_{28} (b_{1g}), ν_{11} (a_g), ν_{19} (b_{1g}), ν_2 (a_g), and ν_{10} (a_g). The occurrence of modes with both a_g and b_{1g} symmetry is attributed to the employed excitation wavelength which is pre-resonant with respect to the *B* absorp-

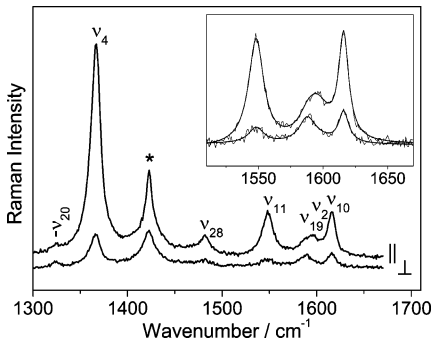

Figure 4. Spontaneous resonance Raman spectra of a ~1 mM solution of MP-IX-DME in CH_2Cl_2 in the region 1300−1670 cm^{-1} obtained with excitation wavelength $\lambda_{exc} = 424.0$ nm; parallel (∥) and perpendicular (⊥) component. Solvent bands are marked with asterisk. The inset displays the baseline-corrected experimental data in the region 1510−1670 cm^{-1} as thin lines together with the results of a least-squares analysis as bold lines.

TABLE 2: Spectral Parameters Determined by a Least-Squares Fitting Procedure for the RR Spectra of MP-IX-DME in the Region 1510−1670 cm^{-1}

$\Omega/2\pi c$/cm^{-1}	A/arb.u.	$\Gamma/2\pi c$/cm^{-1}	ρ^{SR}	ν_i (sym./D_{2h})
1548	2.0	14	0.15	ν_{11} (a_g)
1588	0.2	15	2.32	ν_{19} (b_{1g})
1595	1.3	24	0.12	ν_2 (a_g)
1616	1.3	9	0.30	ν_{10} (a_g)

tion band; RR spectra acquired with strict *B* band resonance conditions are usually solely dominated by totally symmetric (a_g) modes, because the resonance enhancement is mainly governed by Albrecht's *A* term in which contributions from nontotally symmetric modes are ineffective.[37,38] In our RR spectra, the absolute intensities of a_g modes are stronger than those of the b_{1g} modes, but the latter are still detected with an intensity that allows a reasonable quantitative determination of the band parameters. Simultaneous curve fitting to the parallel and perpendicular spectra was performed in the region 1510−1670 cm^{-1} (inset of Figure 4) to enable a direct comparison to the coherent Raman spectra covering the same range. In this region, spectral contributions of four macrocycle modes are detected; the corresponding band parameters determined from the least-squares fit to the spontaneous RR spectra are listed in Table 2. For the given excitation wavelength, the overall amplitudes *A* of the totally symmetric modes ν_{11}, ν_2, and ν_{10} are higher than that of the nontotally symmetric mode ν_{19}. In particular, the depolarization ratios (ρ^{SR}) are helpful for an unambiguous mode assignment due to their symmetry dependency: the totally symmetric modes are polarized with depolarization ratios close to $^1/_8$ (ν_{11}, ν_2) or $^1/_3$ (ν_{10}), while the nontotally symmetric vibration ν_{19} exhibits an anomalous polarization ($\rho^{SR} = 2.3$); this clearly separates the a_g modes from the b_{1g} mode. The smaller difference in ρ^{SR} observed among the totally symmetric modes also occurred in a comparable study on the fully symmetrically substituted OEP;[12] therefore, this difference cannot be attributed to specific symmetry deviations in MP-IX-DME.

Polarization-Sensitive Resonance CARS Spectroscopy. The coherent Raman spectra were measured with a double electronic resonance condition as indicated in Figure 1. The pump laser wavelength of $\lambda_L = 625.7$ nm is pre-resonant with respect to the $Q_x(00)$ electronic absorption, and the generated anti-Stokes continuum, $\Delta\lambda_{AS}$, is resonant to the $Q_x(01)$ absorption. In the applied frequency-degenerate CARS process that follows the energy conservation rule $\omega_{AS} = 2\omega_L - \omega_S$, therefore, couplings with both eigenstates, $Q_x(00)$ and $Q_x(01)$, may contribute to

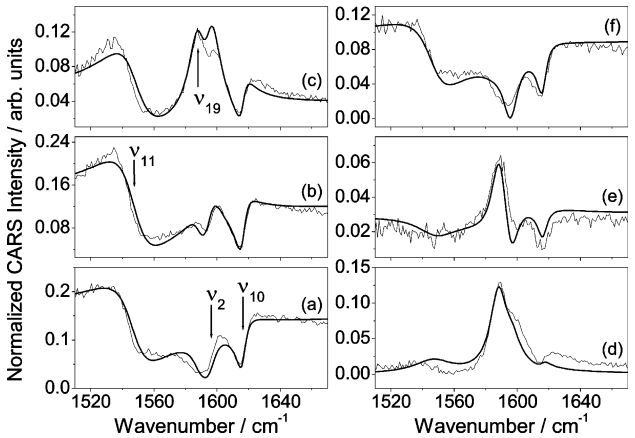

Figure 5. PS resonance CARS spectra of a ~5 mM solution of MP-IX-DME in CH_2Cl_2 in the region 1510−1670 cm^{-1} obtained with a pump wavelength $\lambda_L = 625.7$ nm and a broad-band Stokes continuum, $\Delta\lambda_S$, centered at ~696.8 nm. The spectra are recorded with analyzer settings $\beta = -30°$ (a), −60° (b), 90° (c), 60° (d), 30° (e), and 0° (f). The normalized experimental spectra are depicted as thin lines, the results of a least-squares fitting procedure using eqs 1 and 2 as bold lines.

TABLE 3: Spectral Parameters Determined by a Least-Squares Fitting Procedure Using Eqs 1 and 2 for the PS RCARS Spectra of MP-IX-DME in the Region 1510−1670 cm^{-1} [a]

$\Omega/2\pi c$/cm^{-1}	A^R/arb.u.	$\Gamma/2\pi c$/cm^{-1}	Θ^R/deg	ρ^R	ν_i (sym./D_{2h})
1547	6.3	29	41	0.79	ν_{11} (a_g)
1588	0.2	13	269	−15	ν_{19} (b_{1g})
1596	6.0	12	94	0.50	ν_2 (a_g)
1616	1.5	8	92	0.49	ν_{10} (a_g)

[a] The value for the nonresonant background is $\chi^{NR} = 1.0$.

enhancement effects. Similar to the RR spectra, modes of both a_g and b_{1g} symmetry can be observed. The normalized CARS spectra of MP-IX-DME in the region 1510−1670 cm^{-1} obtained for six different polarization arrangements are displayed in Figure 5 along with curves fitted according to eqs 1 and 2.

A stable minimum in the simultaneous least-squares fit to all six spectra was obtained by assuming the same four bands that were also detected in the *B* band resonance Raman spectra (cf. inset of Figure 4). The resulting parameter set is listed in Table 3. Apart from the positions (Ω), amplitudes (A), line widths (Γ), and depolarization ratios (ρ) that are also accessible in spontaneous Raman spectroscopy, the coherent spectra additionally contain the coherent phase (Θ) of the signal waves. In several studies on metalloporphyrins[8,10] and free-base porphyrins,[12] the values of Θ^R correlated to the mode symmetry and may therefore, together with the depolarization ratio, serve as a symmetry marker. In Table 3, modes with similar depolarization ratios ρ^R also exhibit similar coherent phases Θ^R. The modes ν_2 and ν_{10}, for example, have depolarization ratios of ~0.5; the phase shift for both modes is around 90° with respect to the phase of the nonresonant background. The mode ν_{11}, whose depolarization ratio is close to $^3/_4$, shows a phase shift of 41°. The coherent phases of all totally symmetric modes (ν_{11}, ν_2, ν_{10}) are significantly separated from the phase of the nontotally symmetric and anomalously polarized vibration ν_{19} with $\rho^R = -15$ and $\Theta^R = 269°$.

The fact that not only b_{1g} modes but also a_g modes appear with considerable intensity in the PS RCARS spectra of MP-IX-DME with Q_x band excitation should be noted here in particular. While a similar behavior was found for the free-base OEP,[12] PS RCARS spectra of metalloporphyrins with

comparable excitation conditions, i.e., pre-resonant $Q(00)$ and resonant $Q(01)$ contributions, are often clearly dominated by nontotally symmetric modes.[9,10] Furthermore, spontaneous RR spectra of OEP with Q_y band excitation only contain significant contributions from ν_{19} (b_{1g}) in the spectral region under discussion.[39] Such changes in the enhancement pattern may be attributed to the symmetries of the electronic states involved in the scattering process; these symmetries are different for free-base porphyrins as compared to metalloporphyrins. In metalloporphyrins the *B* and *Q* states are both of E_u symmetry, and *x*- and *y*-polarized transitions are indistinguishable. Due to symmetry lowering ($D_{4h} \rightarrow D_{2h}$), in free-base porphyrins the *B* and *Q* bands are split into an *x* component with B_{3u} symmetry and a *y* component with B_{2u} symmetry.[39] It has already been mentioned above that *B* band RR spectra are usually dominated by a scattering process described by Albrecht's *A* term, which generally favors the enhancement of totally symmetric modes. For *Q* band resonant spectra, however, scattering due to Albrecht's *B* term becomes relevant. For *B* term scattering, especially, those modes which are effective in coupling *B* and *Q* electronic states gain intensity in the Raman spectra.[2,38] Our Raman spectroscopic results indicate that totally symmetric modes in free-base porphyrins are more effective for vibronic couplings than they are in metalloporphyrins. Discussing such coupling mechanisms in detail, however, is not the scope of this paper.

Comparison of Spontaneous and Coherent Raman Spectra. From the band parameters determined in the CARS experiments, hypothetical polarized spontaneous Raman spectra can be reconstructed;[10,12] this enables a direct comparison between the *B* band RR spectra and the *Q* band RCARS spectra. For this purpose, the positions (Ω), amplitudes (A), and line widths (Γ) from the coherent spectra can be directly employed for the reconstruction of the spontaneous spectra. In the case of the depolarization ratios, however, the different definitions for the spontaneous (ρ^{SR}) and coherent (ρ^{R}) cases and consequently the different dependency from corresponding tensor invariants must be considered:

$$\rho^{SR} \equiv \frac{I_{\perp}^{SR}}{I_{\parallel}^{SR}} = \frac{3\bar{g}^2 + 5\bar{g}_A{}^2}{45\bar{a}^2 + 4\bar{g}^2} \tag{3}$$

$$\rho^{R} \equiv \frac{\chi_{1221}^{(3)R}}{\chi_{1111}^{(3)R}} = \frac{3\bar{\gamma}^2 - 5\bar{\gamma}_A{}^2}{45\bar{\alpha}^2 + 4\bar{\gamma}^2}. \tag{4}$$

Here, $\bar{a}^2$, $\bar{g}^2$, and $\bar{g}_A{}^2$ are the isotropic, anisotropic, and antisymmetric invariants of the Raman polarizability tensor; $\bar{\alpha}^2$, $\bar{\gamma}^2$, and $\bar{\gamma}_A{}^2$ are the corresponding invariants for the third-order susceptibility tensor. For our simulations, the correlation between ρ^{SR} and ρ^{R} for a_g and b_{1g} modes in the D_{2h} point group is of relevance. For totally symmetric modes, in general, the antisymmetric invariants vanish ($\bar{g}_A{}^2 = \bar{\gamma}_A{}^2 = 0$), and the relation $\rho^{SR} = \rho^{R}$ holds. For b_{1g} (D_{2h}) modes, however, the isotropic invariants vanish ($\bar{a}^2 = \bar{\alpha}^2 = 0$), while the anisotropic and antisymmetric invariants do not.[31] As a consequence, a direct relation between ρ^{SR} and ρ^{R} is not generally possible. In the particular case of ν_{19} (b_{1g}), however, we conclude $5\bar{\gamma}_A{}^2 \gg 3\bar{\gamma}^2$, because of its strongly negative CARS depolarization ratio ρ^{R} (cf. eq 4). Therefore, in the following simulation of spontaneous Raman spectra, we assumed $\rho^{SR} = -\rho^{R}$ as an approximation for this b_{1g} mode. In the simulation, Lorentzian line shape functions are used for each band.

A comparison between the spontaneous and coherent Raman spectra of MP-IX-DME is illustrated in Figure 6; the left panel

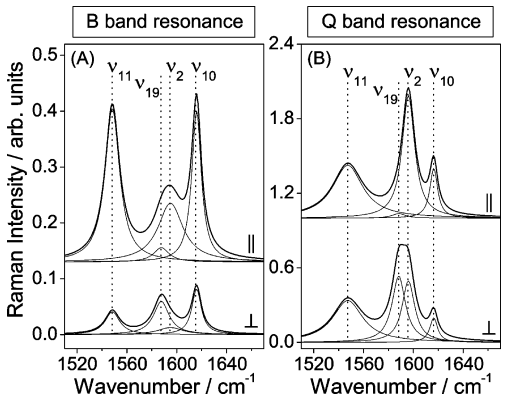

Figure 6. Comparison of polarized Raman spectra for *B* and *Q* band resonance conditions. (A) Simulated spectra employing the parameters in Table 2 (bold lines), representing the best fit to the experimental spontaneous RR spectra. Individual bands are depicted as thin lines. (B) Simulated spectra employing the parameters in Table 3 (bold lines), representing hypothetical spontaneous Raman spectra measured with *Q* band excitation. Individual bands are depicted as thin lines. The parallel components in (A) and (B) are vertically shifted for clarity.

reflects the best fit to the experimental polarized RR spectra, and the right panel shows the corresponding spectra simulated with the parameters obtained by the line shape analysis of the PS RCARS spectra. This visualizes the major differences in relative enhancements of the amplitudes, in line widths, and in depolarization ratios that occur by changing the excitation condition from *B* to *Q* band resonance. Concerning the intensity enhancement and the line widths, the modes ν_{11} and ν_2 show the most obvious differences. Their amplitude is relatively increased in comparison to the amplitude of ν_{10} (cf. Tables 2 and 3); furthermore, a significant broadening of the ν_{11} band and a narrowing of the ν_2 band are observed, while the line widths of ν_{10} and ν_{19} remain nearly constant. Differences in line widths may on one hand be attributed to the different lifetimes of the electronic states involved in the scattering processes, but may on the other hand also strongly depend on the different experimental conditions employed in the RR and RCARS measurements. More attention should be payed to the changes in depolarization ratios which may be particularly sensitive to the mode symmetry. In an early resonance Raman study on MP-IX-DME,[24] where the excitation wavelength was tuned over the $Q_y(01)$ absorption region, it was found that throughout the whole excitation range ν_{11} and ν_{10} remain polarized with depolarization ratios $\rho < 0.5$ and ν_{19} remains anomalously polarized; no statement is made about ν_2. For the Q_x excitation applied in our RCARS experiments, ν_{19} (b_{1g}) still remains anomalously polarized. The depolarization ratios for the three investigated totally symmetric modes, however, are recognizably increased in comparison to the spectra with $Q_y(01)$ band excitation up to a value of $\rho = 0.79$ in the case of ν_{11}. This suggests that the depolarization ratio dispersion, which is expected in the range $0 < \rho^{SR} < 0.75$ for b_{1g} (D_{2h}) modes,[40] shows a tendency toward higher values with decreasing excitation energies.

Comparison to Octaethylporphine (OEP). The results presented for MP-IX-DME will in the following be compared to a similar study on OEP performed by us recently.[12] Since the experimentally applied excitation wavelengths are the same for MP-IX-DME and OEP and the respective electronic absorption spectra of both molecules also show no significant differences, we consider it justified to directly compare the corresponding Raman band parameters; the similarity of absorption properties in the Q_x band region, which is relevant for the

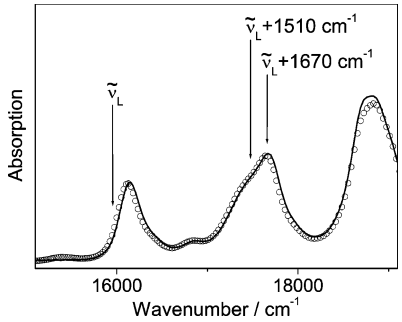

Figure 7. Comparison between the absorption spectra of OEP (line) and MP-IX-DME (circles) in the spectral region that is relevant for the RCARS measurements. The absolute wavenumbers of the pump laser ($\tilde{\nu}_L$) and of the anti-Stokes signal range are indicated.

TABLE 4: Comparison of Selected Band Parameters of MP-IX-DME and OEP (in square brackets) for Spectra Measured with Identical Excitation Conditions[a]

$\Omega/2\pi c$/cm^{-1} [b,c]	ρ^{SR} [c]	ρ^{R} [c]	Θ^{R} [c]	ν_i (sym./D_{2h})
1548 [1545]	0.15 [0.19]	0.79 [0.77]	41 [39]	ν_{11} (a_g)
1588 [1587]	2.3 [4.9]	−15 [−7.3]	269 [253]	ν_{19} (b_{1g})
1595 [1589]	0.12 [0.12]	0.50 [0.80]	94 [81]	ν_2 (a_g)
1616 [1614]	0.30 [0.31]	0.49 [0.58]	92 [67]	ν_{10} (a_g)

[a] ρ^{SR} is determined with pre-resonant *B* band excitation and ρ^{R}, Θ^{R} with Q_x band excitation. Parameters for OEP are adopted from ref 12. [b] Values taken from the spontaneous *B* band RR spectra. [c] Errors estimated from measurements on test molecules (cf. Experimental Section): ±1 cm^{-1} ($\Omega/2\pi c$); ±0.05 (ρ^{SR} of ν_{11}, ν_{10}); ±0.15 (ρ^{R} of ν_{11}, ν_2, ν_{10}); ±15 (Θ^{R}). Errors for ρ^{SR} of ν_{19}, ν_2 and ρ^{R} of ν_{19} may be larger.

CARS measurements, is illustrated in Figure 7. In the following, wavenumber values, depolarization ratios, and coherent phases are discussed. These parameters are summarized in Table 4 for both molecules.

In MP-IX-DME, all modes appear at slightly increased wavenumbers; the most significant difference of 6 cm^{-1} occurs for ν_2. The modes in the region above 1400 cm^{-1} are conveniently used as marker bands for the porphyrin core size;[2] in addition, correlations of Raman wavenumbers to certain bond lengths and angles have been found in previous studies.[41] If the degree of planarity is kept, higher wavenumbers correspond to a smaller core size.[41] Quite obvious shifts in wavenumbers often occur in metalloporphyrins for different complexation[42] or exchange[9,41] of the metal atom while, for example, the substitution at the C_m atoms causes less pronounced effects.[43] By comparing the four modes investigated here for MP-IX-DME and OEP, one can conclude that a change in the β substitution pattern affects the Raman band positions by even smaller amounts. The increased wavenumbers in MP-IX-DME may indicate a slight decrease in core size compared to OEP. From the quantum chemical calculations described above, however, no significant deviations in the geometry of both molecules were detected. This suggests that effects of the β substitution on the porphyrin core either do not exist or lie in a range that is beyond the accuracy of the calculated values, or are due to solvent effects not covered in our gas-phase calculations.

The depolarization ratios and the coherent phases represent the parameters that are expected to be especially sensitive to symmetry alterations. As can be seen from Table 4, however, these parameters exhibit nearly the same tendencies in OEP as in MP-IX-DME. With the accuracy criteria for the measurements taken into account, the mode ν_{11} (a_g) shows identical behavior in both molecules. For the modes ν_{19} (b_{1g}), ν_2 (a_g), and ν_{10} (a_g), some small differences between the OEP and MP-IX-DME Raman spectra can be recognized. For example, the anomalous polarization of ν_{19} (b_{1g}) is increased in the *Q* band spectra of MP-IX-DME, the polarized mode ν_2 (a_g) tends to a slightly lower value of ρ^{R}, and for ν_{10} (a_g), the value of Θ^{R} is slightly increased in the MP-IX-DME spectra.

Like the normal-mode calculations presented above, the examination of the linear and nonlinear Raman spectroscopic data again confirms that the influence of the β substitution pattern on the macrocycle symmetry is very small. Nevertheless, slight variations of some parameters are detected. From the four modes investigated, ν_2 seems to be most effectively influenced by the different β substitution pattern, revealing obvious differences in wavenumber positions as well as depolarization ratios; in contrast, the mode ν_{11} appears to be rather insensitive, especially with regard to symmetry-specific parameters.

4. Conclusions

We have presented an investigation of four macrocycle modes (ν_{11}, ν_{19}, ν_2, ν_{10}) of MP-IX-DME in the region 1510−1670 cm^{-1} by means of polarized resonance Raman (RR) spectroscopy, polarization-sensitive resonance CARS (PS RCARS) spectroscopy, and DFT calculations; we compared the results to former studies on OEP[11,12] with the intention of detecting possible influences of the different β substitution pattern on the macrocycle geometry and/or the symmetry of the vibrational modes. The DFT calculations on MP-IX-DME did not reveal any significant effects of the β substituents on the macrocycle geometry but indicated that the normal-mode coordinates of the four investigated vibrations slightly deviate from an ideal D_{2h} symmetric behavior; this is an effect that could not be recognized in a previous calculation on OEP.[11] Accurate band parameters for these vibrations were determined by curve fitting to polarized pre-resonant *B* band Raman spectra and to PS CARS spectra measured with a double Q_x band resonance condition. The analysis of both sets of spectra and a direct comparison between them revealed major differences in depolarization ratios and coherent phases between the a_g modes (ν_{11}, ν_2, ν_{10}) and the b_{1g} mode (ν_{19}); some smaller differences were observed among the a_g modes. The considerable activity of a_g modes in the Q_x band spectra of MP-IX-DME was noted in particular, because this behavior is uncommon as compared to metalloporphyrin spectra with *Q* band excitation or free-base porphyrin spectra with Q_y band excitation.

The band positions, depolarization ratios, and coherent phases determined for MP-IX-DME were compared to corresponding parameters determined for OEP in a previous study that was carried out with identical excitation conditions.[12] Several subtle differences between the two molecules were identified. Among the investigated vibrational modes, ν_2 exhibited the largest differences in Raman band parameters.

In summary, we have shown that the unsymmetric β substitution pattern in MP-IX-DME, even if it does not introduce a recognizable distortion of the macrocycle geometry, has subtle effects on the symmetry of specific normal modes. It has been demonstrated that sensitive Raman techniques in combination with DFT-derived normal-mode data provide the ability to describe even such small differences. Furthermore, the application of coherent Raman spectroscopy allowed us to accomplish excitation conditions that are not accessible by spontaneous Raman spectroscopy because the latter would be obscured by fluorescence signals. CARS spectroscopy is therefore ideally suited for investigating the resonance behavior of free-base porphyrins in the *Q* band absorption region. The quantitatively evaluated RCARS data we presented may also serve as a basis

to interpret two-dimensional femtosecond CARS spectra where the signal is resolved in both wavenumber and time domain. Corresponding investigations have been made on OEP, MgOEP, and MgTPP.[44−46] By taking into account recent developments toward an improved spectral resolution in femtosecond CARS experiments,[47] these techniques are also suitable to probe small structural differences in large biomolecules.

Acknowledgment. Financial support from the German Research Foundation (Deutsche Forschungsgemeinschaft, Sonderforschungsbereich 630, Teilprojekt C1) is gratefully acknowledged.

References and Notes

(1) Shelnutt, J. A.; O'Shea, D. C. *J. Chem. Phys.* **1978**, *69*, 5361.
(2) Spiro, T. G. *Adv. Protein Chem.* **1985**, *37*, 111.
(3) Schick, G. A.; Bocian, D. F. *Biochim. Biophys. Acta* **1987**, *895*, 127.
(4) Schweitzer-Stenner, R. *Q. Rev. Biophys.* **1989**, *22*, 381.
(5) Igarashi, R.; Adachi, Y.; Maeda, S. *J. Chem. Phys.* **1980**, *72*, 4308.
(6) Apanasevich, P. A.; Kvach, V. V.; Orlovich, V. A. *J. Raman Spectrosc.* **1989**, *20*, 125.
(7) de Boeij, W. P.; Lucassen, G. W.; Otto, C.; Greve, J. *J. Raman Spectrosc.* **1993**, *24*, 383.
(8) Voroshilov, A.; Otto, C.; Greve, J. *J. Chem. Phys.* **1997**, *106*, 2589.
(9) Nissum, M.; Funk, J.-M.; Kiefer, W. *J. Raman Spectrosc.* **1999**, *30*, 605.
(10) Otto, C.; Voroshilov, A.; Kruglik, S. G.; Greve, J. *J. Raman Spectrosc.* **2001**, *32*, 495.
(11) Schlücker, S.; Koster, J.; Nissum, M.; Popp, J.; Kiefer, W. *J. Phys. Chem. A* **2001**, *105*, 9482.
(12) Koster, J.; Popp, J.; Schlücker, S. *J. Raman Spectrosc.* **2006**, *37*, 384.
(13) Hamaguchi, H. *J. Chem. Phys.* **1977**, *66*, 5757.
(14) Akhmanov, S. A.; Bunkin, A. F.; Ivanov, S. G.; Koroteev, N. I. *Sov. Phys. JETP* **1978**, *47*, 667.
(15) Koroteev, N. I.; Endemann, M.; Byer, R. L. *Phys. Rev. Lett.* **1979**, *43*, 398.
(16) Brakel, R.; Schneider, F. W. In *Advances in Spectroscopy*; Clark, R. J. H., Hester, R. E., Eds.; John Wiley: Chichester, 1988; Vol. 15, Chapter 4, p 149.
(17) Zheltikov, A. M. *J. Raman Spectrosc.* **2000**, *31*, 653.
(18) Saito, Y.; Ishibashi, T.; Hamaguchi, H. *J. Raman Spectrosc.* **2000**, *31*, 725.
(19) Ujj, L.; Atkinson, G. H. In *Handbook of Vibrational Spectroscopy*; Chalmers, J. M., Griffths, P. R., Eds.; John Wiley: Chichester, 2002; Vol. 1, p 585.
(20) Kozlowski, P. M.; Jarzęcki, A. A.; Pulay, P. *J. Phys. Chem.* **1996**, *100*, 7007.
(21) Kozlowski, P. M.; Jarzęcki, A. A.; Pulay, P.; Li, X.-Y.; Zgierski, M. Z. *J. Phys. Chem.* **1996**, *100*, 13985.
(22) Jarzęcki, A. A.; Spiro, T. G. *J. Phys. Chem. A* **2005**, *109*, 421.
(23) Verma, A. L.; Bernstein, H. J. *Biochem. Biophys. Res. Commun.* **1974**, *57*, 255.
(24) Plus, R.; Lutz, M. *Spectrosc. Lett.* **1975**, *8*, 119.
(25) Venkateshrao, S.; Yin, J.; Jarzęcki, A. A.; Schultz, P. G.; Spiro, T. G. *J. Am. Chem. Soc.* **2004**, *126*, 16361.
(26) Frisch, M. J.; Trucks, G. W.; Schlegel, H. B.; Scuseria, G. E.; Robb, M. A.; Cheeseman, J. R.; Montgomery, J. A., Jr.; Vreven, T.; Kudin, K. N.; Burant, J. C.; Millam, J. M.; Iyengar, S. S.; Tomasi, J.; Barone, V.; Mennucci, B.; Cossi, M.; Scalmani, G.; Rega, N.; Petersson, G. A.; Nakatsuji, H.; Hada, M.; Ehara, M.; Toyota, K.; Fukuda, R.; Hasegawa, J.; Ishida, M.; Nakajima, T.; Honda, Y.; Kitao, O.; Nakai, H.; Klene, M.; Li, X.; Knox, J. E.; Hratchian, H. P.; Cross, J. B.; Bakken, V.; Adamo, C.; Jaramillo, J.; Gomperts, R.; Stratmann, R. E.; Yazyev, O.; Austin, A. J.; Cammi, R.; Pomelli, C.; Ochterski, J. W.; Ayala, P. Y.; Morokuma, K.; Voth, G. A.; Salvador, P.; Dannenberg, J. J.; Zakrzewski, V. G.; Dapprich, S.; Daniels, A. D.; Strain, M. C.; Farkas, O.; Malick, D. K.; Rabuck, A. D.; Raghavachari, K.; Foresman, J. B.; Ortiz, J. V.; Cui, Q.; Baboul, A. G.; Clifford, S.; Cioslowski, J.; Stefanov, B. B.; Liu, G.; Liashenko, A.; Piskorz, P.; Komaromi, I.; Martin, R. L.; Fox, D. J.; Keith, T.; Al-Laham, M. A.; Peng, C. Y.; Nanayakkara, A.; Challacombe, M.; Gill, P. M. W.; Johnson, B.; Chen, W.; Wong, M. W.; Gonzalez, C.; Pople, J. A. *Gaussian 03*, revision C.02; Gaussian, Inc.: Wallingford, CT, 2004.
(27) Kiefer, W.; Bernstein, H. J. *Appl. Spectrosc.* **1971**, *25*, 500.
(28) Knoll, P.; Singer, R.; Kiefer, W. *Appl. Spectrosc.* **1990**, *44*, 776.
(29) Funk, J.-M.; Michelis, T.; Eck, R.; Materny, A. *Appl. Spectrosc.* **1998**, *52*, 1541.
(30) Toleutaev, B. N.; Tahara, T.; Hamaguchi, H. *Appl. Phys. B* **1994**, *59*, 369.
(31) Kamisuki, T.; Takeuchi, S.; Akamatsu, N.; Adachi, Y.; Maeda, S. *J. Chem. Phys.* **1988**, *88*, 4592.
(32) Kleinman, D. A. *Phys. Rev.* **1962**, *126*, 1977.
(33) Spiro, T. G.; Kozlowski, P. M.; Zgierski, M. Z. *J. Raman Spectrosc.* **1998**, *29*, 869.
(34) Little, R. G.; Ibers, J. A. *J. Am. Chem. Soc.* **1975**, *97*, 5363.
(35) Parthasarathi, N.; Hansen, C.; Yamaguchi, S.; Spiro, T. G. *J. Am. Chem. Soc.* **1987**, *109*, 3865.
(36) Li, X.-Y.; Zgierski, M. Z. *J. Phys. Chem.* **1991**, *95*, 4268.
(37) Albrecht, A. C. *J. Chem. Phys.* **1961**, *34*, 1476.
(38) Perrin, M. H.; Gouterman, M.; Perrin, C. L. *J. Chem. Phys.* **1969**, *50*, 4137.
(39) Sato, S.; Kitagawa, T. *Appl. Phys. B* **1994**, *59*, 415.
(40) McClain, W. M. *J. Chem. Phys.* **1971**, *55*, 2789.
(41) Sparks, L. D.; Anderson, K. K.; Medforth, C. J.; Smith, K. M.; Shelnutt, J. A. *Inorg. Chem.* **1994**, *33*, 2297.
(42) Choi, S.; Spiro, T. G.; Langry, K. C.; Smith, K. M.; Budd, L. D.; La Mar, G. N. *J. Am. Chem. Soc.* **1982**, *104*, 4345.
(43) Li, X.-Y.; Czernuszewicz, R. S.; Kincaid, J. R.; Su, Y. O.; Spiro, T. G. *J. Phys. Chem.* **1990**, *94*, 31.
(44) Heid, M.; Chen, T.; Schmitt, U.; Kiefer, W. *Chem. Phys. Lett.* **2001**, *334*, 119.
(45) Heid, M.; Schlücker, S.; Schmitt, U.; Chen, T.; Schweitzer-Stenner, R.; Engel, V.; Kiefer, W. *J. Raman Spectrosc.* **2001**, *32*, 771.
(46) Schmitt, M.; Heid, M.; Schlücker, S.; Kiefer, W. *Biopolymers* **2002**, *67*, 226.
(47) Kano, H.; Hamaguchi, H. *Appl. Phys. Lett.* **2005**, *86*, 121113/1.